ESA Climate Change Initiative

aerosol_cci

LMD Dust properties retrieval Algorithm Theoretical Basis Document (ATBD)

Version 2.1

DOCUMENT STATUS SHEET

	FUNCTION	NAME	DATE	SIGNATURE
LEAD AUTHOR	editor	Virginie Capelle		
CONTRIBUTING AUTHORS		Alain Chédin		
REVIEWED BY	Co-Science Leader	Gerrit de Leeuw	24.04.2017	
APPROVED BY	Technical officer (ESA)			
ISSUED BY	Project manager			

EXECUTIVE SUMMARY

The method for the retrieval of dust characteristics from IASI observations was originally developed for application to AIRS (Pierangelo et al., 2004, 2005), and slightly modified as described in detail in Peyridieu et al., 2010, 2013 and in Capelle et al., 2014. It is a three-step algorithm based on a "Look-Up-Table" (LUT) approach. LUTs are computed for a large selection of atmospheric situations from the climatological data base "Thermodynamic Initial Guess Retrieval" (TIGR) (Chédin et al., 1985; Chevallier et al., 1998). All radiative transfer simulations are carried out using the fast line-by-line Automatized Atmospheric Absorption Atlas "4A/OP" model (Scott and Chédin, 1981), in its "OPerational version", coupled to the discrete ordinate algorithm (DISORT) (Stamnes et al., 1988) to account for dust particle scattering (http://ara.abct.lmd.polytechnique.fr/ and http: //www.noveltis.net/4AOP/). The first step determines the atmospheric state observed; the second step simultaneously determines the aerosol 10 μm AOD and mean layer altitude. The third step determines the dust coarse mode effective radius following the approach described in Pierangelo et al. (2005). "Radius-LUT" are built for a set of representative effective radius values using a Mie code (Mishchenko et al., 2002). Several aspects of the retrieval algorithm: robustness to aerosol model (size distribution, shape, and refractive indices), possible contamination by other aerosol species, radiative transfer model bias removal, or cloud mask including discrimination between clouds and aerosols, etc., were investigated and details may be found, for example, in Pierangelo et al., 2004, and, more recently in Capelle et al., 2014.

Issue	Date	Modified Items / Reason for Change
1.0	17.11.2014	
1.2	18.11.2015	Update 2nd year of Aerosol_cci, see Section 7.2.3
2.1	18.04.2017	Update 3rd year of Aerosol_cci, see Section 7.2.3

LIST OF TABLES

LIST OF FIGURES

TABLE OF CONTENTS

1 INTRODUCTION

1.1 Scope

This document describes the theoretical basis for dust aerosol retrieval algorithm developed by LMD for the IASI (Infrared Atmospheric Sounding Interferometer) instruments developed by CNES (French Space Agency) on board of ESA-EUMETSAT Metop satellites.

1.2 References

1.2.1 Applicable Documents

[AD1] Statement of Work "ESA Climate Change Initiative Stage 1, Scientific user Consultation and Detailed Specification", ref EOP-SEP/SOW/0031-09/SP. Issue 1.4, revision 1, dated 9 November, 2009, together with its Annex C "Aerosols" (altogether the SoW).

[AD2] The Prime Contractor's Baseline proposal, ref. 3003432, Revision 1.0, dated 16 June 2010, and the minutes of the July 26, 2010 kick-off meeting

1.2.2 Reference Documents

[RD1] Forster, P., Ramaswamy, V., Artaxo, P., Berntsen, T., Betts, R., Fahey, D. W., Haywood, J., Lean, J., Lowe, D. C., Myhre, G., Nganga, J., Prinn, R., Raga, G., Schulz, M., and Van Dorland, R.: Radiative Forcing of Climate Change, in Climate Change 2007: The Physical Science Basis. Contribution of Working Group I to the Fourth Assessment Report of the Intergovernmental Panel on Climate Change, edited by S. Solomon, D. Qin, M. Manning, Z. Chen, M. Marquis, K. B. Averyt, M. Tignor, and H. L. Miller, pp. 129–234, Cambridge Univ. Press, Cambridge, United Kingdom and New York, NY, USA, 2007.

[RD2] U.S. Climate Change Science Program: Atmospheric aerosol properties and climate impacts, A report by the U.S. Climate Change Science Program and the Subcommittee on Global Change Research, edited by Chin, M., Kahn, R. A., and Schwartz, S. E., report, 128 pp., NASA, Washington, D. C., 2009.

[RD3] Hansen, J., Sato, M., and Ruedy, R.: Radiative forcing and climate response. J. Geophys. Res., 102, 6831-6864, doi:10.1029/96JD03436, 1997.

[RD4] Kaufman, Y. J., Tanre, D., Gordon, H. R., Nakajima, T., Lenoble, J., Frouin, R., Grassl, H., Hermann, B. M., King, M. D., and Teillet, P. M.: Passive remote sensing of tropospheric aerosol and atmospheric correction for the aerosol effect, J. Geophys. Res., 102(D14), 16,815–16,830, doi:10.1029/97JD01496, 1997.

[RD5] Haywood, J. M., and Ramaswamy, V.: Global sensitivity studies of the direct radiative forcing due to anthropogenic sulfate and black carbon aerosols, J. Geophys. Res., 103(D6), 6043–6058, doi:10.1029/97JD03426, 1998.

[RD6] Claquin, T., Schulz, M., Balkanski, Y., and Boucher, O.: Uncertainties in assessing radiative forcing by mineral dust, Tellus B, 50, no. 5, 491–505, 1998.

[RD7] Sokolik, I. N. and Toon, O. B.: Incorporation of mineralogical composition into models of the radiative properties of mineral aerosol from UV to IR wavelengths. J. Geophys. Res., 104, 9423–9444, 1999.

[RD8] Myhre, G. and Stordal, F.: Global sensitivity experiments of the radiative forcing due to mineral aerosols, J. Geophys. Res., 106, No. D16, 18193–18204, 2001.

[RD9] Tanré, D., Haywood, J., Pelon, J., L´eon, J.-F., Chatenet, B., Formenti, P., Francis, P., Goloub, P., Highwood, E., and Myhre, G.: Measurement and modeling of the Saharan dust radiative impact: Overview of the Saharan Dust Experiment (SHADE), J. Geophys. Res., 108(D18), 8574, doi:10.1029/2002JD003273, 2003.

[RD10] Yu, H., Kaufman, Y. J., Chin, M., Feingold, G., Remer, L. A., Anderson, T. L., Balkanski, Y., Bellouin, N., Boucher, O., Christopher, S., DeCola, P., Kahn, R., Koch, D., Loeb, N., Reddy, M. S., Schulz, M., Takemura, T., and Zhou, M.: A review of measurement-based assessments of the aerosol direct radiative effect and forcing, Atmos. Chem. Phys., 6, 613–666, doi:10.5194/acp-6-613-2006, 2006.

[RD11] Otto, S., de Reus, M., Trautmann, T., Thomas, A., Wendisch, M., and Borrmann, S.: Atmospheric radiative effects of an in situ measured Saharan dust plume and the role of large particles, Atmos. Chem. Phys., 7, 4887–4903, doi:10.5194/acp-7-4887-2007, 2007

[RD12] Müller, D., Lee, K.-H., Gasteiger, J., Tesche, M., Weinzierl, B., Kandler, K., Müller, T., Toledano, C., Otto, S., Althausen, D., and Ansmann, A.: Comparison of optical and microphysical properties of pure Saharan mineral dust observed with AERONET Sun photometer, Raman lidar, and in situ instruments during SAMUM 2006, J. Geophys. Res., 117, D07211, doi:10.1029/2011JD016825, 2012.

[RD13] Ryder, C. L., Highwood, E. J., Rosenberg, P. D., Trembath, J., Brooke, J. K., Bart, M., Dean, A., Crosier, J., Dorsey, J., Brindley, H., Banks, J., Marsham, J. H., McQuaid, J. B., Sodemann, H., and Washington, R.: Optical properties of Saharan dust aerosol and contribution from the coarse mode as measured during the Fennec 2011 aircraft campaign, Atmos. Chem. Phys., 13, 303-325, doi:10.5194/acp-13-303-2013, 2013.

[RD14] Legrand, M, Bertrand, J. J., Desbois, M., Menenger L., Fouquart, Y. : The potential of infrared satellite data for the retrieval of saharan-dust optical depth over Africa, J. Appl. Meteorol., 28-4, 309-319, doi: 10.1175/15200450, 1989.

[RD15] Pierangelo, C., Chédin, A., Heilliette, S., Jacquinet-Husson, N., and Armante, R.: Dust altitude and infrared optical depth from AIRS, Atmos. Chem. Phys., 4, 1813-1822, doi:10.5194/acp-4-1813-2004, 2004.

[RD16] Pierangelo, C., Mishchenko, M.,Balkanski, Y. and Chédin, A.: Retrieving the effective radius of Saharan dust coarse mode from AIRS, Geophys. Res. Lett., 32, L20813, doi:10.1029/2005GL023425, 2005.

[RD17] De Souza-Machado, S., Strow, L. L., Motteler, H., and Hannon, S.: Infrared dust spectral signatures from AIRS, Geophys. Res. Lett., 33, L03801, doi:10.1029/2005GL024364, 2006.

[RD18] Peyridieu, S., Chédin, A., Tanré, D., Capelle, V., Pierangelo, C., Lamquin, N., and Armante, R.: Saharan dust infrared optical depth and altitude retrieved from AIRS: a focus over North Atlantic – comparison to MODIS and CALIPSO, Atmos. Chem. Phys., 10, 1953-1967, doi:10.5194/acp-10-1953-2010, 2010.

[RD19] Klüser, L., Martynenko, D., Holzer-Popp, T.: Thermal infrared remote sensing of mineral dust over land and ocean: a spectral SVD based retrieval approach for IASI. Atmos. Meas. Tech. 4, 757e773. doi:10.5194/amt-4-757, 2011.

[RD20] Klüser, L., Kleiber, P., Holzer-Popp, T., Grassian, V. H.: Desert dust observation from space- Application of measured mineral component infrared extinction spectra, Atmos. Environ.,54, 419-427, 2012.

[RD21] Peyridieu S., Chédin A., Capelle V., Tsamalis C., Pierangelo C., Armante R., Crevoisier C., Crépeau L., Siméon M., Ducos F., Scott N.A. : Characterization of dust aerosols in the infrared from IASI and comparison with PARASOL, MODIS, MISR, CALIOP, and AERONET observations., Atmos. Chem. Phys., 13, 6065-6082 doi:10.5194/acp-13-6065-2013, 2013.

[RD22] Capelle V., Chédin A., Siméon M., Tsamalis C., Pierangelo C., Pondrom M., Armante R., Crevoisier C., Crépeau L. and Scott. N.A., Evaluation of IASI derived dust aerosols characteristics over the tropical belt. Atmos. Chem. Phys. , 14, 9343-9362 doi:10.5194/acp-14-9343-2014 (2014)

[RD23] Chiapello, I., G. Bergametti, G., Gomes, L., Chatenet, B., Dulac, F., Pimenta, J., and Santos Suares, E.: An additional low layer transport of Sahelian and Saharan dust over the North-Eastern Tropical Atlantic, Geophys. Res. Lett., 22, 3191–3194, 1995

[RD24] Chiapello, I., Moulin, C., and Prospero, J. M.: Understanding the long-term variability of African dust transport across the Atlantic as recorded in both Barbados surface concentrations and large-scale Total Ozone Mapping Spectrometer (TOMS) optical thickness, J. Geophys. Res., 110, D18S10, doi:10.1029/2004JD005132, 2005.

[RD25] Tsamalis, C., Chédin, A., Pelon, J., and Capelle, V.: The seasonal vertical distribution of the Saharan Air Layer and its modulation by the wind, Atmos. Chem. Phys., 13, 11235-11257, 2013.

[RD26] Pierangelo, C. : in “Aerosol Remote Sensing”, J. Lenoble, L. Remer, and D. Tanré, Eds., Chapter 9, Springer-Praxis Books: Environmental Sciences, 510pp, ISBN-13: 9783642174407, 2013.

[RD27] Maher, B. A., Prospero, J. M., Mackie, D., Gaiero, D., Hesse, P. P., and Balkanski, Y.: Global connections between aeolian dust, climate and ocean biogeochemistry at the present day and at the last glacial maximum, Earth-Science Reviews, 99, 61–97, doi: 10.1016/j.earscirev.2009.12.001, 2010.

[RD28] Mahowald, N. M., Kloster, S., Engelstaedter, S., Moore, J. K., Mukhopadhyay, S., McConnell, J. R., Albani, S., Doney, S. C., Bhattacharya, A., Curran, M. A. J., Flanner,

M. G., Hoffman, F. M., Lawrence, D. M., Lindsay, K., Mayewski, P. A., Neff, J., Rothenberg, D., Thomas, E., Thornton, P. E., and Zender, C. S.: Observed 20th century desert dust variability: impact on climate and biogeochemistry, Atmospheric Chemistry and Physics, 10, 10 875–10 893, doi:10.5194/acp-10-10875-2010, 2010.

[RD29] Formenti, P., Schütz, L., Balkanski, Y., Desboeufs, K., Ebert, M., Kandler, K., Petzold, A., Scheuvens, D., Weinbruch, S., and Zhang, D.: Recent progress in understanding physical and chemical properties of African and Asian mineral dust, Atmos. Chem. Phys., 11, 8231–8256, doi:10.5194/acp-11-8231-2011, 2011.

[RD30] Shao, Y., Wyrwoll, K., Chappell, A., Huang, J., Lin, Z., McTainsh, G. H., Mikami, M., Tanaka, T. Y., Wang, X., and Yoon, S.: Dust cycle: An emerging core theme in Earth system science, Aeolian Research, 2, 181–204, doi:10.1016/j.aeolia.2011.02.001, 2011.

[RD31] Knippertz, P., and Todd, M. C.: Mineral dust aerosols over the Sahara: Meteorological controls on emission and transport and implications for modeling, Rev. Geophys., 50, RG1007, doi:10.1029/2011RG000362, 2012.

[RD32] Markowicz, K. M., Flatau, P. J., Vogelmann, A. M., Quinn, P. M., and Welton, E.: Influence of relative humidity on aerosol radiative forcing: An ACE-Asia experiment perspective. J. Geophys. Res., 108, 8662, doi:10.1029/ 2002JD003066, 2003

[RD33] Vogelmann, A. M., Flatau, P. J., Szczodrak, M., Markowicz, K. M., and Minnett, P. J.: Observations of large aerosol infrared forcing at the surface, Geophys. Res. Lett., 30, 1655, doi:10.1029/2002GL016829, 2003.

[RD34] Scott, N.A. and Chédin, A.: A fast line-by-line method for atmospheric absorption computations: The Automatized Atmospheric Absorption Atlas. J. Appl. Meteor., 20, 802-812, 1981.

[RD35] Stamnes, K., Tsay, S.-C., Wiscombe, W., and Jayaweera, K.: Numerically stable algorithm for discrete ordinate-method radiative transfer in multiple scattering and emitting layered media, *Appl. Optics, 27*, 2502–2509, 1988.

[RD36] Chédin, A., Scott, N. A., Wahiche, C., and Moulinier, P.: The improved initialisation inversion method: A high resolution physical method for temperature retrievals from satellites of the TIROS-N series, J. Clim. Appl. Meteorol., 24, 128–143, 1985..

[RD37] Chevallier, F., Chéruy, F., Scott, N. A., and Chédin, A.: A neural network approach for a fast and accurate computation of a longwave radiative budget, J. Appl. Meteorol., 37, 1385–1397, 1998.

[RD38] Chandrasekhar, S., Radiative Transfer (New York: Dover), 1960.

[RD39] Hansen, J.E., and L.D. Travis: Light scattering in planetary atmospheres. Space Sci. Rev., 16, 527-610, doi:10.1007/BF00168069, 1974.

[RD40] Heilliette S., A. Chedin, N.A. Scott, R. Armante, Parametrization of the effect of surface reflection on spectral infrared radiance measurements. Application to IASI, JQRST 06/2004; 86(2):201-214 2004.

[RD41] Mishchenko, M. I., Travis, L. D., and Lacis, A. A.: Scattering, Absorption, and Emission of Light by Small Particles, Cambridge University Press, Cambridge, 2002

[RD42] Dubovik, O., Holben, B., Eck, T.F., Smirnov, A., Kaufman, Y.J., King, M.D., Tanré, D. and Slutsker, I. : Variability of Absorption and Optical Properties of Key Aerosol Types Observed in Worldwide Locations. *J. Atmos. Sci.* 59: 590–608, 2002.

[RD43] Sokolik, I., Toon, O. B., and Bergstrom, R.W.: Modeling the radiative characteristics of airborne mineral aerosols at infrared wavelengths, J. Geoph. Res., 103(D8), 8813–8826, 1998.

[RD44] Capelle, V., Chédin, A., Péquignot, E.,Schlüssel, P., Newman, S. M., and Scott, N. A. : Infrared continental surface emissivity spectra and skin temperature retrieved from IASI observations over the tropics. J. Appl. Meteor. Climatol., 51, 1164-1179, doi:10.1175/JAMC-D-11-0145.1, 2012.

[RD45] Hess, M., Koepke, P., and Schult, I.: Optical Properties of Aerosols and Clouds: The software package OPAC, Bull. Am. Met. Soc., 79, 831–844, 1998.

[RD46] Volz, F. E.: Infrared optical constants ammonium sulfate, Sahara dust, volcanic pumace and flyash, *Applied Optics,* 12, 564-568, 1973.

[RD47] Carlson, T. N., and Benjamin, S. G.: Radiative heating rates for Saharan dust. J. Atmos. Sci. 37, 193–213, 1980.

[RD48] Balkanski, Y., Schulz, M., Claquin, T., and Guibert, S.: Reevaluatio of Mineral aerosol radiative forcings suggests a better agreement with satellite and AERONET data, Atmos. Chem. Phys., 7, 81–95, doi:10.5194/acp-7-81-2007, 2007.

[RD49] Fouquart, Y., B. Bonnel, G. Brogniez, J. Buriez, L. Smith, J. Morcrette, and A. Cerf: Observations of Saharan aerosols: Results of ECLATS field experiment. Part II: Broadband radiative characteristics of the aerosols and vertical radiative flux divergence. J. Climate Appl. Meteor., 26, 38–52, 1987.

[RD50] Volz, F. E., Infrared refractive index of atmospheric aerosol substances, Appl. Opt., 11, 755–759, doi:10.1364/AO.11.000755 (1972).

[RD51] Wahiche C., Scott N.A.,Chédin A.: Cloud detection and cloud parameters retrievals from the satellites of the Tiros-N series. Annales Geophysicae, 43, pp. 207-222., 1986

[RD52] Crevoisier C., Heilliette S., Chédin A., Serrar S., Armante R., Scott N.A.: Midtropospheric CO2 concentration retrieval from AIRS observations in the tropics. Geophys. Res. Lett., 31, L17106, doi:10.1029/2004GL020141, 2004.

2 IASI INSTRUMENT CHARACTERISTICS

Developed by CNES in collaboration with EUMETSAT, the IASI instrument (Chalon et al., 2001; http://smsc.cnes.fr/IASI), onboard the ESA-EUMETSAT MetOp-A polar platforms, is a Fourier Transform Spectrometer that measures Earth-emitted infrared radiation. Launched in October 2006 and operational since July 2007, it provides 8461 spectral channels, between 15.5 µm (645 cm-1) and 3.63 µm (2755 cm-1) with a spectral resolution of 0.50 cm−1 after apodisation, and a regular spectral sampling interval of 0.25 cm−1. MetOp-A crosses the Equator at 9:30 p.m., Local Time (LT), on its ascending node. IASI provides a near global coverage twice a day at a spatial resolution of 12 km at nadir.

3 SCOPE OF THE PROBLEM

3.1. Motivation and Constraints

During the past decades, determination of atmospheric aerosol characteristics from space has been extensively done using instruments measuring in the visible part of the spectrum. This has greatly contributed enhancing knowledge of the aerosol impact on the Earth radiation balance (direct effect) as well as on the clouds (albedo, lifetime) (indirect effect). However, these processes are complex as they involve the aerosol distribution (spatial, in particular vertical, and temporal), and their microphysical and optical properties (size, shape, composition, etc.). Moreover, the accuracy obtained on the atmospheric radiative effect also depends on surface characteristics (albedo, temperature). This complexity still leads to large uncertainties in the estimation of aerosols impact on climate (e.g. [RD1]-[RD13]).
After a long period of relative lack of interest in aerosol remote sensing in the infrared (one of the oldest reference is by [RD14]), a marked growing interest in the infrared is now observed with the emergence of hyperspectral instruments as AIRS and IASI ([RD15]-[RD22]). Coarse mode aerosols have a higher contribution to infrared radiation compared to fine mode aerosols. Dust and sea-salt particles are the main components of the coarse mode, the latter usually remaining in the planetary boundary layer, at which altitudes infrared radiances collected at satellite level show poor sensitivity. Most of mineral dust aerosol mass is composed of particles in the coarse size mode, thus with a potentially high optical depth in the infrared, and can be brought to high altitudes in the atmosphere, for example in the so-called Saharan Air Layer ([RD23],[RD24],[RD25]). Consequently, the remote sensing of aerosols in the longwave domain mostly focuses on retrievals of mineral dust properties ([RD26]). This domain offers some unique opportunities such as nighttime aerosol observation, the determination of the aerosol layer mean altitude or the aerosol characterization over deserts. Mineral dust is a major contributor to total aerosol loading and has been the subject of an increasing number of studies (e.g. [RD27]-[RD31]) due, in particular, to its potentially large contribution to atmospheric radiative forcing ([RD32],[RD33],[RD11]). Visible wavelengths are sensitive to both fine and coarse mode particles when infrared wavelengths are essentially sensitive to the coarse mode. Associating these two spectral domains should help improving our knowledge of the impact of aerosols on climate, its variability and evolution. This requires validating infrared-derived aerosol properties using well recognized, accurate and independent, measurements of these properties, as well as understanding possible differences brought by such comparison.

3.2. General approach

The method used to derive dust characteristics from IASI observations is a three-step algorithm based on a “Look-Up-Table” (LUT) approach ([RD15], [RD16,] [RD18,] [RD21]). The first step determines the atmospheric state observed; the second step determines simultaneously the 10 µm AOD and the aerosol layer mean altitude, while the dust coarse mode effective radius is determined in the third step.

For each steps, Look-Up-Tables of IASI simulated brightness temperatures are calculated using the forward coupled radiative transfer model 4A/OP-DISORT (RD34], [RD35]; http://4aop.noveltis.com). Entries to the model include: AOD, altitude, surface pressure, surface temperature and emissivity, viewing angle, and a set of 2311 atmospheric situations, selected by statistical methods from 80,000 radiosonde reports, and stored in the "TIGR" (Thermodynamic Initial Guess Retrieval) climatological data base ([RD36],[RD37]). Each situation is described, from the surface to the top of the atmosphere, by the values of the temperature, water vapour and ozone concentrations on a given pressure grid.

4. SCIENTIFIC BACKGROUND

4.1. Forward radiative transfer model with scattering process

Contrary to radiative transfer in shortwave domain, where the sun is the only source of radiation, in longwave domain, the main source of radiation is the Earth. The observed radiation is emitted by the Earth's surface and/or by the atmospheric layers. It is partly absorbed by the molecules and aerosols and/or scattered by the aerosols: it thus contains the signature of the atmosphere.

Let us assume that the electromagnetic wave propagates in the direction (θ,φ) and let $\mu=cos(\theta)$. In a scattering medium of single scattering albedo ϖ and phase function p, the differential form of the radiative transfer equation (RTE) can be written, under the hypothesis of local thermodynamic equilibrium, as:

$$\frac{dI_\upsilon(t,\mu,\varphi)}{dt} = -\frac{1}{t} I_\upsilon(t,\mu,\varphi) + \frac{1-\varpi}{t} B_\upsilon(T(t)) + \frac{\omega}{(4\pi)t} \int_0^{2\pi}\int_{-1}^{1} p(t;\mu,\varphi;\mu',\varphi') I(t,\mu',\varphi') d\mu' d\varphi' \quad (1)$$

Where I_ν is the spectral radiance emitted by the atmosphere at frequency ν, $B_\nu(T(t))$ the Planck function that describes the spectral radiance of the radiation emitted at frequency ν by a blackbody at temperature T at time t (see for example [RD26]).

If solar radiation from direction (θ_s,φ_s) cannot be dismissed (e.g. for shorter wavelength up to 4 µm during daytime), then a fourth term must be added to the previous equation:

$$J_{sun} = \frac{\varpi}{(4\pi)t} I_{sun}\, p(t;\mu,\varphi;\mu_s,\varphi_s) t^{\mu/\mu_s} \quad (2)$$

where I_{sun} is the solar radiance at the top of the atmosphere and $\mu_s=1/cos(\theta_s)$ is negative.

The RTE is thus an integro-differential equation with no analytical solution. In our case, the numerical solution of the RTE equation is computed with the forward coupled radiative transfer model 4A/OP-DISORT ([RD34],[RD36]; http://4aop.noveltis.com) that combines 4A/OP line-by-line model (required by the very thin spectral lines of molecules and the very high spectral resolution of infrared sounders) and the scattering algorithm DISORT (Discrete ordinate algorithm, first described by [RD37]) or SOS (successive orders of scattering) algorithm (e.g. [RD38];[RD39]). The line-by-line model that computes the absorption by the atmosphere requires as input the temperature at every level of the atmosphere, as well as the concentration of all species involved in the absorption at a given frequency and also surface parameters such as the surface temperature, pressure and emissivity. The DISORT or SOS scattering codes require the gaseous optical depth profile (given by the line-by-line absorption code) and aerosol parameters. The scattering parameters (extinction, single scattering albedo and phase function) are needed at each vertical level and are estimated using a Mie code

given a size distribution and a refractive index ([RD40] and ftp://ftp.giss.nasa.gov/pub/crmim/spher.f).

4.2. Impact of atmospheric and surface properties

The two main difficulties when dealing with aerosol in infrared domain are:

- Radiance (or more commonly used its equivalent brightness temperature) sensitivity to aerosol properties is of second order behind the impact of atmospheric temperature, water vapor and surface state.

- The impact of the aerosol depends strongly on the atmospheric situation.

This is illustrated Figure 4.2-1 (top) which shows histograms of the brightness temperature at 965.5 cm^{-1} for about 600 tropical atmospheric situations of TIGR (top). One can see that the impact of the atmospheric situation may be as large as 30K. Corresponding histograms of the sensitivity of the brightness temperature to aerosols (10µm AOD of 0.4 at an altitude of 2700 m) are also displayed Figure 4.2-1 (bottom) and show a much more modest impact of +/-4K. Both figures also illustrate the impact of the surface emissivity: from 0.98 (blue) to 0.8 (red).

This implies that the thermodynamic state of the atmosphere and the surface properties have to be known precisely before retrieving aerosol properties or have to be retrieved simultaneously.

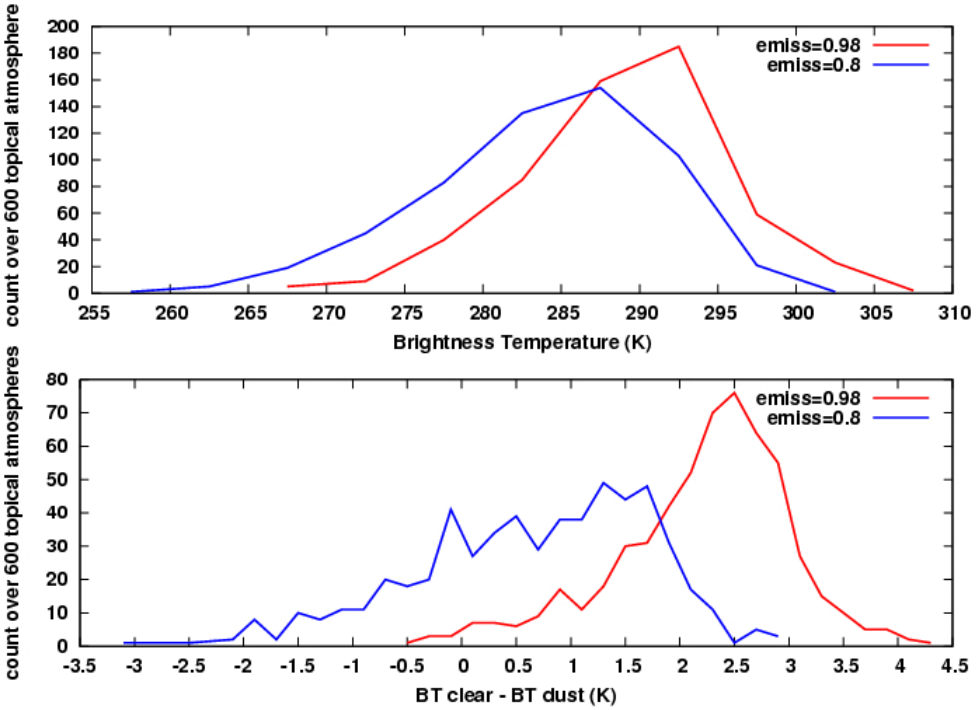

Figure 4.2-1: Histograms of the brightness temperature at 965.5 cm^{-1} for about 600 tropical atmospheric situations of TIGR (top); corresponding histograms of the sensitivity of the brightness temperature to aerosols (10µm AOD of 0.4 at an altitude of 2700 m) (bottom). Both figures also illustrate the impact of the surface emissivity: from 0.98 (blue) to 0.8 (red).

4.3. Impact of micro-physical parameters

The parameters describing aerosol optical properties are the extinction coefficient, directly linked to the AOD, the single scattering albedo, and the asymmetry parameter. These parameters enter the radiative transfer equation for computing radiances or, equivalently, brightness temperatures (BT). These optical properties may be obtained from the a priori knowledge of the aerosol microphysical properties (size distribution and effective radius, refractive indices) using a Lorenz-Mie algorithm (e.g. [RD40]). When studying dust in the infrared domain, the size distribution can be modelled by a monomodal lognormal distribution (see, for example, [RD41]) described by the effective radius (r_{eff}) and the standard deviation of the distribution σ_g. In the following, σ_g stands for $\ln(\sigma_g)$. This approximation is justified by the fact that, if we only consider the dust coarse mode, the contribution of the fine mode in the longwave domain is less than 10% ([RD26], chap 9).

In order to quantify the impact of microphysical parameters on infrared brightness temperatures, difference in BT with a reference case is computed for a relatively high AOD of 0.4 at 10 µm and for an aerosol layer at a mean altitude of 2700m. The reference configuration corresponds to the averaged values seen in the AERONET database: a width of the size distribution of σ_g=0.65, reff=2 µm, refractive index of MITR (from the OPAC database ([RD45]), resulting from the measurements by [RD46], slightly modified by [47] and representative of desert dust far from the sources). Figure 4.3-1 displays the sensitivity of

the IASI brightness temperature to a variation of ±25% of the effective radius reff (top-left), a variation of ±25% of the standard deviation σg (top-right), a change of the refractive index (bottom-left), and a variation of the AOD (bottom-right). Channels used in the inversion are reported as black lines. Four refractive index models are investigated: MITR; "dust-like" from [RD46],[RD50], also in OPAC more representative of non desert mineral aerosols generated from soil, "Revisited" proposed by [RD48] in an effort to reevaluate mineral aerosol radiative forcings, and "Fouquart" from Saharan dust measurements above Niger (Volz cited by [RD49]).

From Figure 4.3-1 we can conclude that the impact of the width of the size distribution σ_g is relatively weak (smaller than 0.1K over the entire spectrum, quite negligible compared to the impact of a variation in AOD (see also e.g. [RD26], chap 9.4). Similar results are obtained for a larger reference 10 µm AOD of 0.6 (impact of 0.2 K instead of 0.1). Concerning the variation of reff (Figure 4.2-1-A), maximum differences are smaller than 0.2 K for an AOD of 0.4 at 10 µm. Note that the impact is proportional to the AOD: at 10 µm, because the AOD is generally not larger than 0.6, the maximum impact is less than 0.5 K for the channel the most sensitive to the size (at 9.3 µm). Indeed, for the channels used in the retrieval, impact is less than 0.3K for an AOD of 0.6. We conclude that, in the infrared domain, the effect of the effective radius is small, particularly on the channels selected. This agrees with [RD42]. Finally, the impact of the refractive index is, by far, the most important. For an AOD of 0.4, the difference in BT can reach 0.8K for two of the channels used in the retrieval (around 12 µm – 830 cm-1). To summarize, for the "reference case" used in this appendix (σg=0.65, reff=2 µm), using OPAC ([RD45]) instead of "Fouquart" can lead to an error of 0.1 for an AOD of 0.4, i.e 25% error. See also the appendix of [RD22] for more details.

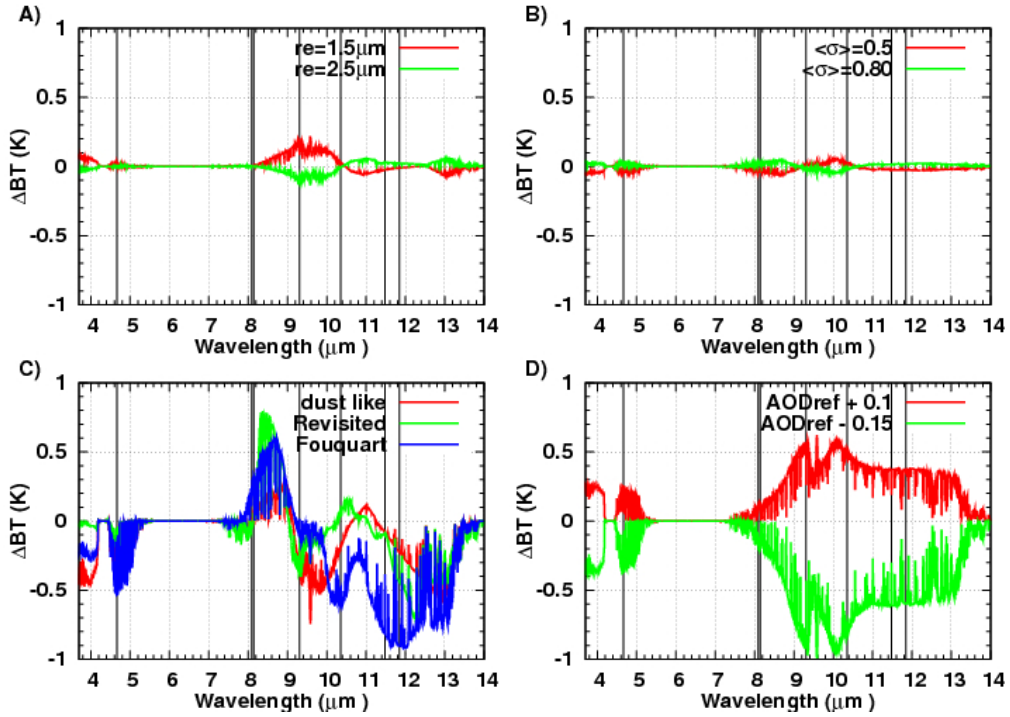

Figure 4.3-1: Sensitivity of IASI brightness temperature to : A) a variation of ±25% of the effective radius reff (here, re); B) a variation of ±25% of the standard deviation σ_g; C) a change in the refractive index (i.e. composition); D) an AOD variation of +0.1 (~25%) and -0.15 (~-37%). Reference conditions: AOD at 10 µm=0.4, mean aerosol layer altitude=2700 m, reff=2µm, σ_g=0.65 and refractive index is MITR.

4.4. Inversion scheme description and definition of the parameterization

Here are defined the different parameters that enter the retrieval procedure. Atmospheric temperature and water vapor profiles, surface temperature, surface pressure and surface emissivity have first to be specified. Some of these parameters are treated as "a priori" knowledge. This is the case of the surface pressure that can be deduced from the altitude of the pixel considered. Surface emissivity is also considered as an a priori known parameter, given the location of the pixel. Indeed, assuming that surface emissivity slowly varies within a month, we use the MSM-IASI surface emissivity 0.5°x0.5° gridded monthly database ([RD43]) retrieved for clear sky pixels. Temperature and water profiles, as well as the surface temperature, are retrieved during the inversion.

Concerning the aerosol properties, we assume that the width of the size distribution has a negligible impact on the retrieval and thus we use a constant value of σ_g=0.65. Concerning the effective radius, we assume a fixed value of 2.3µm for the retrieval of optical depth and altitude. Once these variables are known, the size can then be improved (see [RD16], [RD21]) in a further step. We have seen that the refractive index is the most important microphysical parameter in the infrared. Use is made in the inversion of two models already described in section 4.3: "Revisited" and "dust-like".

In order to take into account all the parameters listed above, we use an approach based on simulated brightness temperature Look-Up-Tables (LUT). All the BT entering the inversion are computed once and for all for a large and representative set of situations (surface characteristics, atmospheric profiles, aerosol characteristics, observation geometry, etc.) and stored in the so-called LUTs. The retrieval process is separated into two parts and two sets of LUTs. First, the atmospheric state is determined using "atmosphere-LUTs" computed without scattering for 18 channels selected to be sensitive to the temperature and water profiles and not sensitive to other species, surface or aerosol properties. Second, the aerosol properties and surface temperature are retrieved from "aerosol-LUTs", corresponding to the atmospheric state determined in the first step, for the 8 channels represented in Figure 4.3-1. These channels combine observations from the medium infrared band (3-4 µm) and the thermal infrared band (8-12 µm), allowing to discriminate aerosol AOD and mean altitude, as their respective impact on the BT may differ ([RD18]).

The retrieval consists in minimizing the normalized distance D between observed and simulated BTs but also BT differences between several couples of channels, here defined for i selected channels and j independent selected couples:

$$D(aod,alt,ts,refr\_ind) = \sum_i \frac{\left(BT_i^{calc} - BT_i^{obs}\right)^2}{\sigma_i^2} + \sum_j \frac{\left(\Delta BT_j^{calc} - \Delta BT_j^{obs}\right)^2}{\sigma_j^2} \quad (3)$$

where σ_i^2 is the variance of the observed BT_i (or ΔBT_i) calculated over the globe for 6 years of IASI measurements (072007-062013). These variances are estimated according the same parameters than those defined in the LUT (viewing angle, surface temperature, surface emissivity, surface pressure, and for three air masses: tropical, midlatitude cold and midlatitude warm. This allows taking into account the natural variability of the observed brightness temperature.

Finally, Ts, AOD and altitude bins for each refractive index are averaged, provided they verify the criterion: $D(AOD, alt,ts,refr\_ind) \leq min(D) \times 1.1 \leq 1$ (4)

5. IMPLEMENTATION

5.1. Creating the LUTs

Entries used to build the IASI simulated brightness temperature LUTs used in are given in Table 5.1-1. In this Table, the entries in bold face correspond to LUTs BTs calculated using the forward coupled radiative transfer model 4A/OP-DISORT. Other entries correspond to LUTs BTs interpolated linearly or quadratically.

Table 5.1-1: Entries used to build the IASI Look-Up-Tables (LUT) of simulated brightness temperatures (BTs) used in the three-step algorithm. BTs for bold-faced values are calculated using the forward coupled radiative transfer model 4AOP-DISORT, BTs for the other values are interpolated (linearly or quadratically).

	step 1 : LUT - Atmosphere	**step 2 : LUT - AOD, altitude**	**step 3: LUT - effective radius**
Number of IASI channels	18	8	1
Angles (°)	**0**, 5, **10**, **15**, **20**, **25**, **30, 35, 40, 45, 50**	**0**, 5, 10, **15**, 20, 25, **30, 35, 40, 45, 50**	**0**, 5, 10, **15**, 20, 25, **30**
Surface pressure	**1013,** 984.20**, 955.12** 927.73**, 900.33**	**1013,** 984.20**, 955.12** 927.73**, 900.33**	**1013,** 984.20**, 955.12** 927.73**, 900.33**
Surface emissivity	**0.60,** 0.65, 0.70, 0.75, **0.80,** 0.85, 0.90, 0.95, **0.98**	**0.60,** 0.65, 0.70, 0.75, **0.80,** 0.85, 0.90, 0.95, **0.98**	**0.60,** 0.65, 0.70, 0.75, **0.80,** 0.85, 0.90, 0.95, **0.98**
Surface temperature	**T(1013mb), T(1013mb)+15K, T(1013mb)-15K (*)**	**T(1013mb), T(1013mb)+15K, T(1013mb)-15K (*)**	**T(1013mb), T(1013mb)+15K, T(1013mb)-15K (*)**
AOD values	N/A	**0.0**, 0.1, 0.2, 0.3, **0.4**, 0.5, 0.6, 0.7, **0.8,** 0.9, 1.0, 1.1, 1.2, 1.3, **1.4**	**0.1**, 0.2, 0.3, **0.4**, 0.5, 0.6, 0.7, **0.8,** 0.9, 1.0, 1.1, 1.2, 1.3, **1.4**
Altitude values (m)	N/A	**757**, **1258**, **1756**, **2411**, **3254**, **4116**, **4965**, **5795**	**757, 1258**, **1756**, **2411**, **3254**, **4116**, **4965**, **5795**
Radii values (μm)	N/A	2.3 (R_{eff}) or 3.0 (r_{modV})	**0.5**, 0.8, **1.0**, **1.5**, **2.0**, 2.5, **3.0**, 4.0, **5.0**
Refractive index	N/A	- "revisited" [RD 48] "dust-like" [RD 46,50]	

(*) For every atmospheric situation, LUTs are computed with 3 surface temperatures: the first corresponds to the temperature at 1013mb, the second and third are this temperature +/-15K. For each pixel considered, the atmospheric state is determined using a first guess surface temperature calculated from a window channel. LUTs are then interpolated to this value using Legendre polynomials. Then, surface temperature is treated as are AOD and altitude.

5.2. Cloud detection

Presence of clouds or aerosols in each IASI pixel is detected by a succession of several multispectral threshold tests, stemming from the detection scheme developed for TOVS ([RD51]) and AIRS ([RD52]). All together, 9 screening tests are used. Among them, 5 tests detect more specifically high and medium clouds using differences between the brightness temperature of IASI and AMSU channels, the latter being almost insensitive to clouds; other tests detect low clouds or aerosols using differences between window channels. All tests are based on threshold values applied to the histograms of each difference. Thresholds depend on the season, the view angle, the surface emissivity, and on the two flags land/sea and night/day.

5.3. Surface emissivity

The largely enhanced capabilities of the second generation sounders, as AIRS or IASI, have led us to develop a new approach, the so-called Multi Spectral Method (MSM), aiming at determining the surface infrared emissivity spectrum from 3.7 to 14 μm at high spectral resolution (here, 0.05 μm), together with the surface temperature, by inverting analytically the radiative transfer equation. The method follows four main steps: (i) an estimation of the atmospheric temperature and water vapor profiles is first obtained through a proximity recognition within the Thermodynamic Initial Guess Retrieval (TIGR) climatological library. With this a priori information, all terms of the radiative transfer equation are calculated by using 4A/OP; (ii) surface temperature is retrieved from observations using a few IASI window channels located around 12 μm and selected for their almost constant emissivity with respect to soil type; (iii) emissivity is then calculated for a set of 101 atmospheric windows (transmittance greater than 0.5) used as hinge-points; (iv) the complete infrared emissivity spectrum at 0.05 μm resolution is finally derived from a combination of the high spectral resolution laboratory spectra of selected materials (MODIS/UCSB and ASTER/JPL emissivity libraries) recognized as the closest to the set of retrieved emissivity values (see [RD44]).
Here use is made of the monthly 0.5°X0.5° grid, assuming that surface emissivity slowly varies within a month.

5.4. Radiative bias removal

Since all the simulations described here depend on the radiative transfer model used, possible systematic biases when applied to real data can exist and have to be removed. These systematic biases can come from the model (e.g. a spectroscopy error) or from the instrument (e.g. calibration uncertainty or insufficient knowledge of the response function). If not corrected, these biases can significantly affect the retrievals. These biases are estimated by comparing statistically simulations and observations for a large set of collocated satellite and radiosonde data. For each IASI channel, the bias is obtained by averaging the difference between simulated (here, computed by the 4A/OP model) and observed brightness temperatures over the whole time period considered. Simulations use collocated radiosondes from the LMD ARSA (Analyzed RadioSoundings Archive) database now covering the period 1979-now (more than 5 million radiosondes archived). These biases, hereafter referred to as “deltacs”, are then added to the observed brightness temperatures.

5.5. Retrieval examples

Figure 5.5-1 displays an example of the LMD IASI retrieval of the 10 µm coarse mode AOD from the 19th to the 22th of March 2010. Retrievals are displayed for no-cloudy scenes and morning overpasses over North Africa.

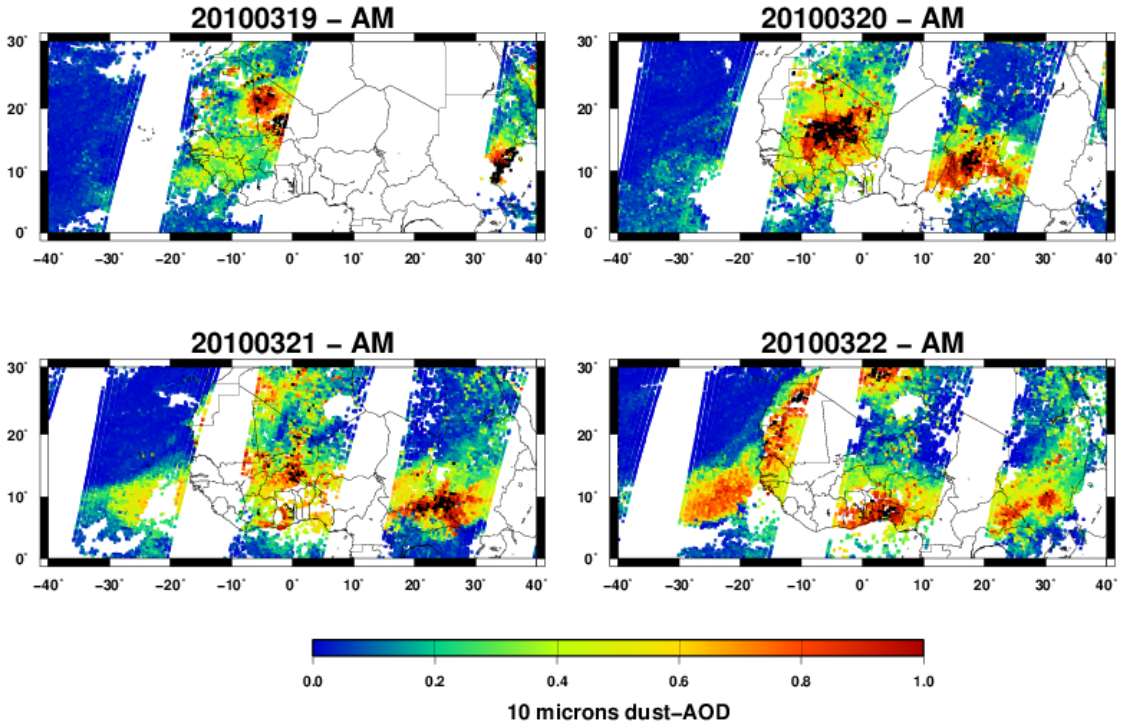

Figure 5.5-1: LMD IASI retrieval of 10µm coarse mode AOD for 4 days in March 2010 (19th to 22th) for no cloudy scenes and for morning overpasses.

6. INPUT DATA REQUIREMENTS

6.1. IASI L1C data

The LMD algorithm requires as spectral inputs the L1c IASI radiance data distributed by EUMETSAT and archived at Ether French data center (http://www.pole-ether.fr).

6.2. Auxiliary data

The auxiliary datasets needed in the algorithm are listed Table 6.2-1

Table 6.2-1: Auxillary data description

Auxillary dataset	Sources	Use in LMD algorithm
Elevation model + land-sea mask	GTOPO30: model (DEM)	elevation model + land-sea mask
AMSU radiances	AMSU radiance data in collocation with IASI	Cloud-mask
MSM-IASI surface emissivity spectrum	Capelle, et al., JAMC, 2012)	Aerosol sensitive channels are also sensitive to surface emissivity

7. ALGORITHM OUTPUT

Output follows the aerosol_cci data formats and naming convention. The list of variables contained from the aerosol_cci LMD algorithm output files is presented in Table 7.1-1.

7.1. Output following the aerosol_cci convention

Table 7.1-1: Dataset names of the aerosol_cci LMD algorithm output files.

Dataset name	Content
"latitude"	Latitude in degrees of FOV center
"longitude"	Longitude in degrees of FOV center
"viewing_zenith_angle"	Viewing zenith angle in degrees for FOV center
"time"	UTC time of observation in decimal hours (HHMMSS)
"AM/PM"	0 =AM/ 1=PM for Morning or evening overpass
"Ocean/land flag"	0=ocean, 1=land
"Cloud flag"	0=no clouds /1 =clouds
"Dust flag"	0=no dust/ 1 = dust / -999=Not sure
"Preretrieval quality flag"	"0=bad, 1=good"
"Postretrieval quality_flag"	QF_{dust} 0=bad, 1=good
"DAOD10000"	Dust $AOD_{10\mu m}$
"DAOD550"	Dust $AOD_{0.55\mu m}$
"DAOD11000"	Dust $AOD_{11\mu m}$
"EAOD10000"	ε_{dust}
"Mean_Altitude"	Dust layer mean altitude (m)
"cloud_mask"	Based upon QF_{cld}

7.2. General remarks regarding the algorithm outputs

7.2.1. Quality flag

Currently, two values of the quality flag are provided by the algorithm. Either the distance defined by Eq. 3 is lower than a threshold value based on the internal variability of the LUT and a value of 10µm coarse mode AOD is provided, or the distance is greater than this threshold and no AOD value is provided. After version1.3, every point flagged as cloud is rejected (and quality flag is set to "bad"). A new filter is added on version 2.1 where quality flag is set to "bad" when AOD>0.06 while the cloud flag indicates clear sky. Further analyses of the distance value and of the resulting AOD standard deviation obtained for each pixel should result in a better quantification of the level of confidence. Work is in progress on this subject.

7.2.2. Dust AOD at 0.55 µm

The algorithm output is the dust AOD at 10µm. As detailed in [RD22], a theoretical conversion ratio between this AOD and its equivalent at 0.55 µm can be estimated from the a priori knowledge of the aerosol microphysical properties (size distribution, effective radius, refractive index), using a Lorenz–Mie calculation. Results show that this ratio strongly varies with both the size distribution and the refractive index. For typical values of the effective radius and width of the size distribution from AERONET, the theoretical ratio may vary between 0.6 and 1.3. Regarding the refractive index (actually, its values at all the channel frequencies used in the algorithm), the theoretical ratio, estimated using the microphysical properties measured by AERONET, may vary from 0.4 for aerosol close to sources to 1.1 for aerosols transported far from the sources. This is a very large range of variation: assuming a different refractive index model can lead to quite a different theoretical ratio. As a consequence, assuming a wrong refractive index leads directly to a bias between infrared and visible AOD. Here, visible AOD estimate is performed during the inversion process, for each situation (i.e. a given set of 10µm AOD, Altitude, surface temperature and refractive index) that satisfies the criterion defined Eq. 4. The ratio thus applied is obtained using σ_g and r_{eff} used to compute the LUT and the corresponding refractive index. The ratio thus obtained is 0.85 for "balkanski et al., 2007" and "1.78" for "dust-like". It must therefore be again emphasized that this conversion is an approximation and can degrade the comparisons made in the visible.

7.2.3. Update in the version v1.2

In version v1.2, a few improvements have been made. The concerned parts of this present ATBD have been updated accordingly. The improvements made are listed below:

- The atmospheric recognition now involves 18 channels compared to the previous 6. This allows a better constraint of the atmosphere.

- The distance used in the proximity recognition is now normalized by the variance of the observed brightness temperature (and no more the calculated one) in order to take only into account the natural variability of the channels involved in the inversion.

- Over arid regions (i.e. where the surface emissivity at 8.55µm is lower than 0.95), two indices are used at the same time in the inversion: "revisited" from [RD 48] and "dust-like" from [RDRD 46,50]. This update impacts mostly the infrared to IR conversion in order to be more in agreement with the observed IR to visible ratio (over sources it was observed that the IR to visible ratio was larger far from sources).

7.2.4. Update in the version v1.3

In this version two major improvements have been applied. This new version has been run for the entire IASI period (from July 2007 to end of 2016):

- Every point flagged as cloud are rejected before inversion

- The proximity recognition are made on the two refractive indices ("revisited" from [RD 48] and "dust-like" from [RDRD 46,50]) for every observed pixel (in the previous section the index "dust-like" was only used over arid regions).

7.2.5. Update in the version v2.1

In this version three major improvements have been applied:

- Iteration on the surface temperature is added. In the first step, the atmospheric profile is constrained using a surface temperature obtained by regression and then a first estimation of the three parameters AOD, altitude and surface temperature is made. In a second step, the entire inversion process is iterated using this new estimation of surface temperature. The iteration stops after a stabilization of the surface temperature (in general below 3 iterations).

- An additional filter is applied when AOD is larger than 0.06 whereas the cloud flag indicates a clear sky pixel. In that case the inversion is rejected.

- The routine is now in parallel mode, running with 20 threads.

8. CONCLUSIONS

This Algorithm Theoretical Basis Document describes the physical basis of the LMD algorithm of aerosol characteristics retrieval in the infrared domain. The document describes the different steps followed in the retrieval, the required inputs, as well as the outputs of the algorithm in the framework of the Aerosol_cci project. It should be mentioned that for this reason, only 10 µm coarse-mode optical depth are in the ouput file whereas the algorithm retrieves simultaneously the mean altitude of the aerosol layer, as well as the surface temperature.

This algorithm has been validated against several other instruments such as MODIS, MISR, PARASOL and AERONET, first at monthly scale [RD18], [RD21], [RD22] and now carried on at daily and IASI pixel scale. The main difficulty met for such comparisons lies in the different instrument measurement time or spatial resolution. Validation work is now evolving towards using data collected during dedicated campaigns, such as FENNEC, that took place in June 2011, and partially in June 2013, on West Africa. Such campaigns not only provide daily measurements of the aerosol properties, but also a precise description of the thermodynamic environement (atmospheric temperature, water vapor, etc.), or of the surface properties (surface temperature, surface emissivity, etc.). Results from these campaigns are crucial to a better understanding of the IASI results and should lead to significant improvements of the algorithm.

End of the document